PCP
PLANT & CELL PHYSIOLOGY

Sorghum bicolor membrane steroid binding protein 1 can bind heme and remodel ER membranes

Khuanpiroon Ratanasopa[1,2,‡], Rocio Ochoa-Fernandez[1,‡], Silas B. Mellor[1,‡], Valentina Travaglia[1], Kasper Hinz[1], Pernille S. Tuelung[3,4] and Tomas Laursen[1,*]

[1]Department of Plant and Environmental Sciences, University of Copenhagen, Thorvaldsensvej 40, 1871 Frederiksberg, Denmark, [2]Department of Immunotechnology, Lund University, Medicon Village, Scheelevägen 2, 221 00 Lund, Sweden, [3]CHPSAXS, Department of Drug Design and Pharmacology, University of Copenhagen, Universitetsparken 2, 2100 København, Denmark, [4]Present address: Ascendis Pharma, A/S, 2900 Hellerup, Denmark

*Corresponding author: E-mail, tola@plen.ku.dk

[‡]Khuanpiroon Ratanasopa, Rocio Ochoa-Fernandez and Silas B. Mellor contributed equally to this work.

Received 25 April 2025; Accepted 29 November 2025

Regular Paper

Abstract

Plant membrane steroid binding proteins (MSBPs) belong to the membrane-associated progesterone receptors (MAPRs), which is present in all eukaryotic kingdoms. Plant MSBPs have been shown to regulate the function of cytochrome P450 enzymes, bind different steroidal compounds and confer salt tolerance. However, the exact molecular function of plant MSBPs remains elusive. Here, we perform a phylogenetic analysis of the six MAPR genes encoded in the *Sorghum bicolor* genome. Of these, four group into a distinct MSBP clade characterized by being N-terminally membrane anchored followed by a cytochrome b_5 domain and an extended disordered C-terminal. Biophysical characterization of SbMSBP1 demonstrates that this protein can bind heme, which leads to dimerization potentially through a heme–heme stacking mechanism. Using untargeted proteomics, We further show that MSBPs are upregulated in both root and shoot tissues upon exposure to salt stress. Based on weighted gene co-expression network analysis, we find that SbMSBP1 abundance clusters with endoplasmic reticulum (ER) remodeling and vesicle transport proteins. We further show that overexpression of SbMSBP1 in *S. bicolor* protoplasts and tobacco results in formation of structures consistent with organized smooth ER. Our data indicate that SbMSBP1 functions to remodel ER membranes, which may be directly linked to a functional role in stress resilience toward both biotic and abiotic stresses and furthermore could serve as a useful tool for metabolic engineering of ER-scaffolded biosynthetic pathways.

Keywords: ER membrane dynamics • organized smooth endoplasmic reticulum • membrane steroid binding protein • salt stress • *Sorghum bicolor* • vesicle transport

Introduction

Membrane steroid binding protein (MSBP) family belongs to the group of membrane-associated progesterone receptors (MAPRs), which are present in all eukaryotic kingdoms (Hehenberger et al. 2020), whose members include Neuferricin (NEUFC) (Kimura et al. 2010a), Neudesin (Kimura et al. 2005), and the most well-characterized mammalian Progesterone Receptor Membrane Component (PGRMC) 1 and 2. Several independent reports indicate that PGRMC1 functions in various cellular processes, such as modulating vesicular trafficking (Ahmed et al. 2010), heme metabolism (Piel III et al. 2016), reticulophagy (Chen et al. 2021), the activity of drug-metabolizing cytochrome P450s, and steroidogenesis (Rohe et al. 2009, Ryu et al. 2017). Hence, the protein plays a crucial role in cell metabolism and cancer biology (You et al. 2021, Lee et al. 2022).

The first structural characterization of human PGRMC1 was the crystal structure of the cytochrome b_5-like domain, which confirmed the conserved fold of this domain (Kabe et al. 2016). The crystal structure revealed that the protein binds heme via a tyrosine residue (Y113) and dimerizes through a heme stacking mechanism. Dimerization of PGRMC1 has been shown to be important for interaction with Epidermal Growth Factor Receptors and cytochrome P450 enzymes (CYP3A4 and CYP1A2) (Kabe et al. 2016). However, a later study showed that binding to PGRMC stabilized P450 in a heme-independent manner (McGuire et al. 2021). Although the mechanism of PGRMC1-mediated stabilization of P450s is currently unknown, multiple studies have confirmed that PGRMC1 binds to P450 enzymes from many families (McGuire et al. 2021).

The MSBP protein family has attracted attention in the plant kingdom based on their role in tolerance toward abiotic challenges such as drought, salinity, and temperature

Plant and Cell Physiology, 2026, 67(3),315–328. https://doi.org/10.1093/pcp/pcaf160, Advance Access publication on 4 December 2025, available online at https://academic.oup.com/pcp

(Witzel et al. 2018, Berka et al. 2020) and biotic stress (Kuhn et al. 2010, von Sivers et al. 2019). The best-characterized plant MAPR proteins are those from *Arabidopsis thaliana*, which harbors four AtMAPR genes (AtMAPR2–5). AtMAPR5, also referred to as Membrane Steroid Binding Protein1 (AtMSBP1), has been demonstrated to bind to progesterone and multiple other steroids with lower affinities *in vitro* (Yang et al. 2005). So far, only a single plant MSBP structure (AtMAPR2) has been solved by nuclear magnetic resonance (NMR) spectroscopy in its apo form (Song et al. 2004).

Previously, AtMSBP1 was shown to play a role in photomorphogenesis, acting as an inhibitor of cell elongation (Yang et al. 2005), indicating that AtMSBP1 plays an essential role in plant growth and development. Later, AtMSBP1 was shown to be involved in brassinosteroid (BR) signaling by enhancing endocytosis of BAK1 [Brassinosteroid Insensitive 1 (BRI1)-Associated Receptor Kinase 1] (Song et al. 2009). Based on these observations, it has been proposed that MSBPs are involved in steroid-related cellular processes (Yang et al. 2008, Shi et al. 2011), though the molecular mechanisms involved in BAK1, BRI1, and AtMSBP1 in endocytosis remain unclear. A direct interaction between AtMSBP1 and an intracellular Qc-SNARE protein, AtBS14b, has been suggested to act as a bridge, enabling the interaction between AtMSBP1 and the extracellular domain of BAK1 and further enhancing endocytosis of BAK1 (Zhu et al. 2014). Most recently, direct interactions were demonstrated between AtMSBP1 and 2 and P450 enzymes involved in lignin biosynthesis in *A. thaliana*, indicating that it also functions as a P450 scaffolding protein (Gou et al. 2018).

In connection with recent studies on cytochrome P450-dependent specialized metabolism in the sub-tropical cop plant *Sorghum bicolor*, we have used styrene maleic acid copolymer to extract discrete lipid particles (SMALPs) (Lee et al. 2016) directly from plant membrane fractions (Smith et al. 2017, Bassard and Laursen 2019). Isolation of the dhurrin biosynthetic enzymes (POR, CYP79A1, and CYP71E1) in SMALPs isolated from sorghum endoplasmic reticulum (ER) revealed a strong enrichment of SbMSBP1 (Laursen et al. 2016). Given the demonstrated effects of MSBP proteins on P450 enzymes, this led us to consider the potential role of SbMSBP1 in sorghum specialized metabolism. Here, we report an overview of sorghum MAPR proteins within a wider phylogenetic comparison of plant MAPR proteins, along with biophysical characterization of SbMSBP1. We confirm that SbMSBP1 is a heme-binding protein with a disordered C-terminus, and that the protein undergoes heme-dependent oligomerization. Using untargeted proteomics of sorghum seedlings exposed to salt stress, we show that the expression of SbMSBP1 is highly correlated with SNARE proteins and other proteins known to be involved in vesicular fusion and vesicle trafficking. By transient expression in sorghum protoplast, we furthermore show that SbMSBP1 localizes to the ER membrane and induces ER-derived vesicle formation. Our findings suggest a potential role of SbMSBP1 in vesicle-mediated transport between subcellular compartments.

Results

Phylogenetic analysis of membrane-associated progesterone receptor family in plants

The genome of *S. bicolor* (L.) Moench contains six genes encoding membrane-associated progesterone receptor (MAPR) proteins. These proteins are all classified as belonging to the Membrane-Associated Progesterone Receptor Component-Related family in the Panther classification system [PTHR10281, (Thomas et al. 2022)], and considered to be closely related to the animal PGRMC proteins. To investigate the evolutionary relationship, we constructed a phylogenetic tree using the 526 sequences classified to this family retrieved from the Panther database (Fig. 1a). This phylogeny reveals three distinct clades of MAPR proteins in plants, designated MSBP clade, c-cup clade, and NEUFC clades, based on Panther subfamily nomenclature. Of these three clades, only proteins belonging to the MSBP clade appear to be membrane anchored, whereas those in the NEUFC clade possess N-terminal signal peptides, and proteins in the c-cup clade comprise only the cytochrome b_5-like domain (Fig. 1b). Besides cytochrome b_5-domain containing proteins, two distant sub-clades grouped into this family are the vacuolar membrane protein clades a and b, which harbor some sequence similarity but have distinct folds based on inspection of alphafold models (not shown). Four of the MAPR protein in *S. bicolor* group in the MSBP clade and will be referred to as SbMSBP1–4, while the c-cup and NEUFC clades contain each one MAPR protein, designated SbMAPR2 to follow *Arabidopsis* nomenclature, and SbNEUFC, respectively (Fig. 1a, Supplementary File 1). The functions of the latter MAPR clades in plants are currently unknown.

SbMSBP1 and other MAPR proteins lack the two histidine residues responsible for coordinating the heme group in classical cytochrome b_5 proteins, and instead shares the canonical residues known to coordinate heme in other MAPR proteins (Fig. 1c). All these sequences share a similar propensity of predicted disordered regions in the $\sim$30 amino acids connecting transmembrane (TM) and cytochrome b_5-like domains, as well as the C-terminus of the protein (Fig. 1d). The amino acid residues in these regions consist mainly of amino acids that are either polar, charged, or only moderately hydrophobic (Ala, Val). A proline-rich linker between the TM domain and cytochrome b_5-like domain appears to be common in the monocot sequences but only partly conserved with *A. thaliana* homologs (Fig. 1c).

Heme binding induces oligomerization of SbMSBP1

To investigate heme binding by SbMSBP1, we first compared heme binding of the full-length protein to that of cytochrome b_5. Purified SbMSBP1 showed a brown color, and showed a spectrum consistent with pentacoordinate heme binding, which was lost upon reduction with dithionite (Supplementary File 1). We next investigated the ability of SbMSBP1 to undergo heme-dependent oligomerization as described for its homologues from human and *Arabidopsis* (Kabe et al. 2016, Gou et al. 2018)

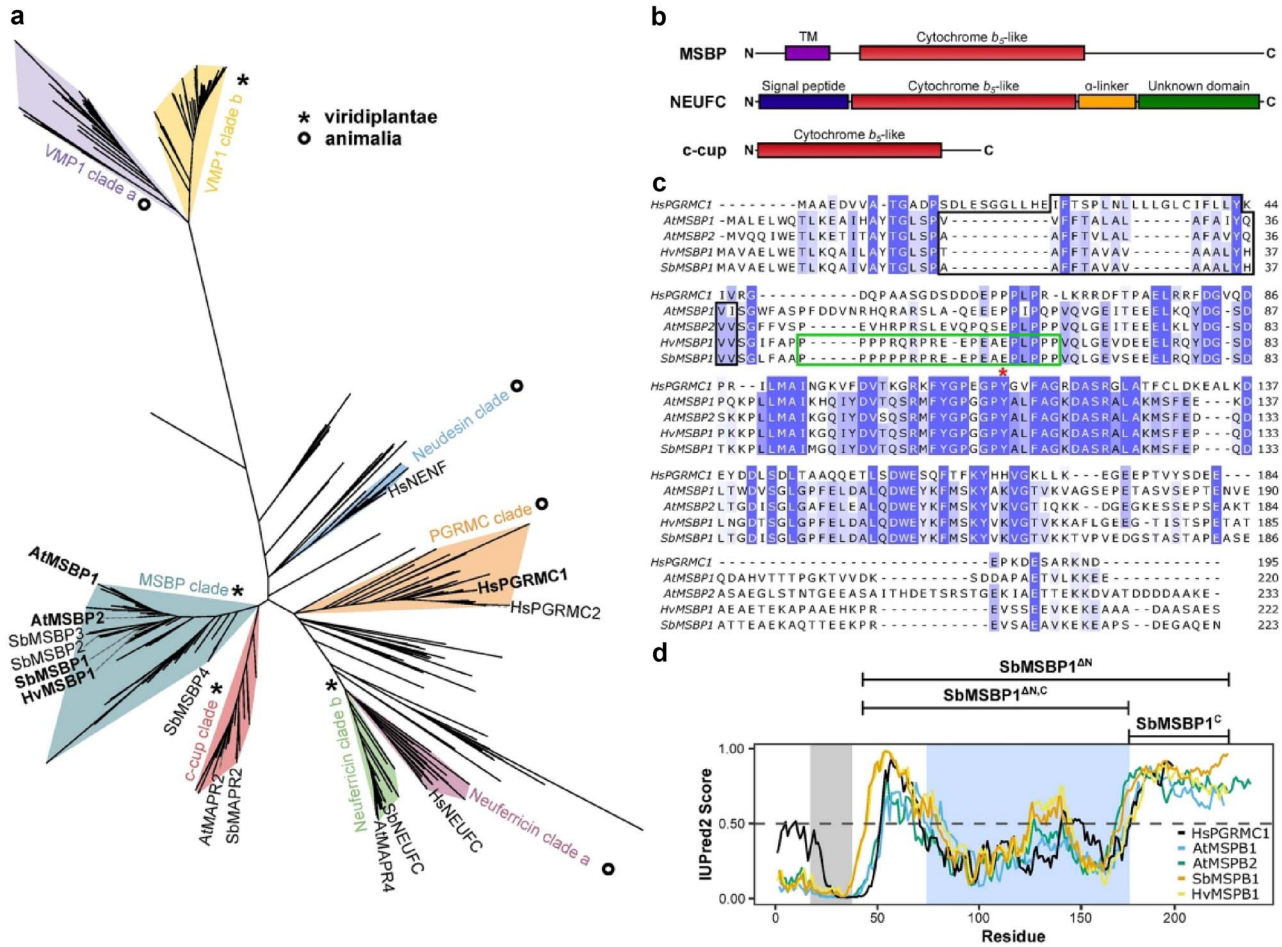

Figure 1. Phylogenetic tree of plant membrane steroid binding proteins (MSBP) and alignment of selected MSBP sequences. (a) Unrooted phylogram of all proteins classified into Panther family PTHR10281. Monophyletic plant and animal clades are colored and indicated by asterisk or open circle, respectively. Sequences used for multiple sequence alignment in (c) are indicated in bold type. (b) Schematic overview of domain structure in plant MAPR protein clades. (c) Multiple sequence alignment of HsPGRMC1, AtMSBP1 and 2, HvMSBP1, and SbMSBP1, performed using MAFFT, with shading to indicate sequence conservation. Predicted TM domains of all proteins and the Pro-rich linker of HvMSBP1 and SbMSBP1 are outlined, with the conserved Tyr residue responsible for heme binding indicated by asterisk. (d) IUPred2 predictions for SbMSBP1, AtMSBP1–2, HvMSBP1, and HsPGRMC1 shows similar overall disorder propensity along the primary sequence. From N- to C-terminus, predicted TM and cytochrome b_5-like domains are shaded. IUPred 2 scores >0.5 indicate disordered sequence, shown by a dashed line. TM, transmembrane domain; NENF, Neudesin; NEUFC, Neuferricin; VMP1, vacuolar membrane protein 1. Residue spans for truncated SbMSBP1 variants used in this study are shown above the plot.

by expressing and purifying the protein without TM domain. We initially prepared a variant missing the TM domain as well as the N-terminal disordered region (residues 1–68, Fig. 1d) but this protein formed gel-like aggregates upon purification that could not be redissolved. To resolve this, we generated a TM-less variant removing residues 1–44 only to retain the N-terminal disordered domain. This variant (referred to as SbMSBP1$^{\Delta N}$) purified as a mixture of apo- and heme-bound forms that could be separated by anion exchange chromatography (Supplementary File 1). Purified apo-SbMSBP1$^{\Delta N}$ produced a similar ferric heme-bound spectrum upon incubation with hemin, as well as dithionite-induced heme dissociation as the full-length protein (Supplementary File 1). Analytical size exclusion chromatography (SEC) showed retention of apo-SbMSBP1$^{\Delta N}$ corresponding to a molecular mass roughly that expected from its sequence (19.4 kDa) (Supplementary File 1). By comparison, the C-terminal disordered domain alone (SbMSBP^{C}) showed a corresponding shift in retention to higher molecular mass equivalent, while an SbMSBP1 variant lacking the TM and C-terminal domains (SbMSBP1$^{\Delta N,C}$, 14.6 kDa) showed good correspondence with expected retention (Supplementary File 1). Performing SEC-MALS produced the expected molecular masses based on refractive index measurements (Supplementary File 1). Together, these SEC-UV and SEC-MALS results indicate that the observed shifts in retention time is likely caused by disorder in the C-terminal domain (Supplementary File 1).

Next, we used SEC-UV to investigate heme-dependent oligomerization by SbMSBP1$^{\Delta N}$. Incubating the protein with increasing hemin concentrations caused a partial retention

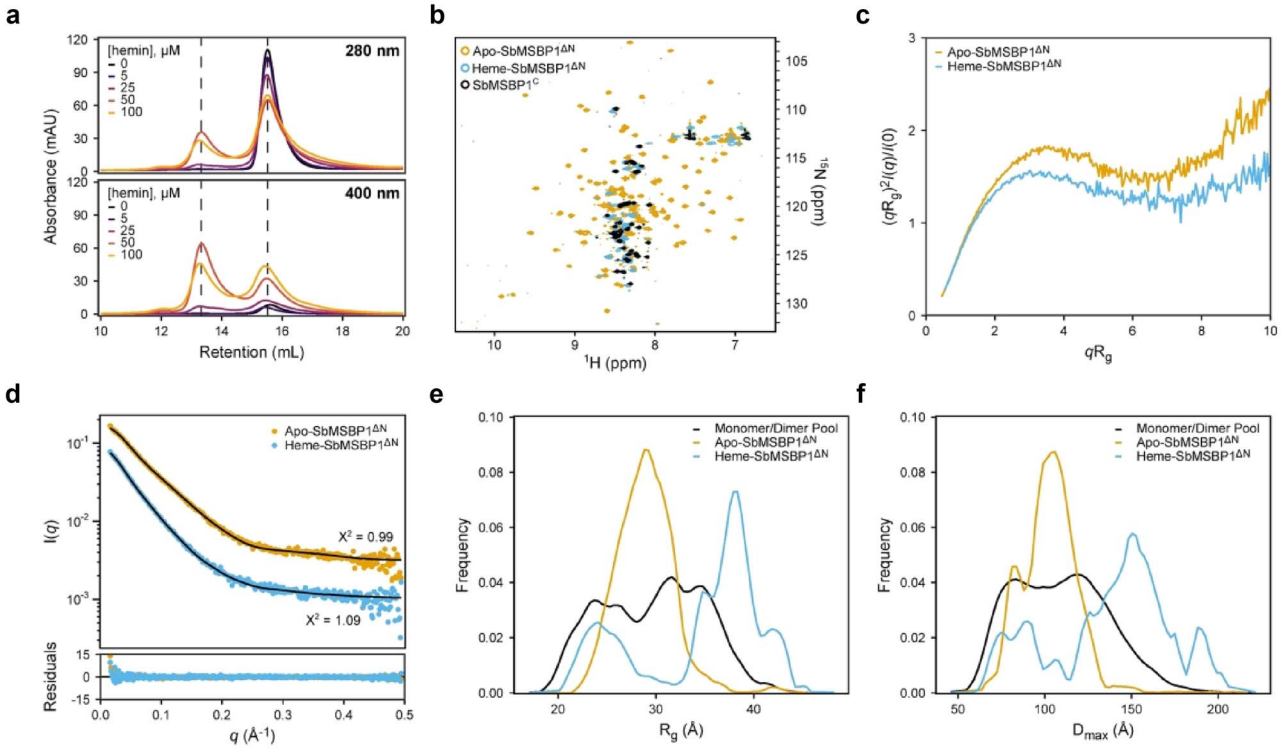

Figure 2. Characterization of SbMSBP1 by SEC-UV and SAXS. (a) Separation of 50 μM apo-SbMSBP1$^{\Delta N}$ on Superdex 200 increase in the presence of increasing hemin concentrations, as detected by UV (top) and hemin Soret absorbance (bottom). (b) ^{1}H-^{15}N-HSQC spectrum of apo-SbMSBP1$^{\Delta N}$ and heme-SbMSBP1$^{\Delta N}$, with the spectrum of SbMSBP^{C} included to show peaks derived from C-terminal residues. (c) Dimensionless Kratky plots of 5 mg mL^{-1} of apo-SbMSBP1$^{\Delta N}$ and heme-SbMSBP1$^{\Delta N}$ suggest a mixture of globular and disordered parts. (d) Ensemble optimization method fits to data at 5 mg mL^{-1} for apo- and heme-SbMSBP1$^{\Delta N}$. Chi-square values are indicated for each fit and normalized fit residuals shown in bottom panel. (e) Rg frequency distributions for apo- and heme-SbMSBP1$^{\Delta N}$ at 5 mg mL^{-1}. (f) D_{max} frequency distributions for apo- and heme-SbMSBP1$^{\Delta N}$ at 5 mg mL^{-1}.

time shift consistent with formation of a higher, hemin-bound oligomeric state (Fig. 2a). Estimates of molecular weight of these oligomers by SEC-MALS was inaccurate due to background scattering from bound heme but suggested the major early eluting peak to be dimeric SbMSBP1$^{\Delta N}$ (Supplementary File 1). 2D ^{1}H-^{15}N-heteronuclear single-quantum coherence (HSQC) NMR showed loss of signal from the cytochrome b_5-like domain of SbMSBP1$^{\Delta N}$ upon heme binding due to paramagnetic peak broadening, whereas the signal corresponding to the C-terminal unstructured domain (residues 175–223) remained broadly unperturbed (Fig. 2b). Together, these results indicate that SbMSBP1$^{\Delta N}$ binds heme and is induced to equilibrate between monomer and oligomeric states *in vitro*. Performing the corresponding experiments with progesterone did not yield detectable oligomerization, nor any observable change in the ^{1}H-^{15}N-HSQC spectrum of SbMSBP1$^{\Delta N}$ (Supplementary File 1).

Small angle X-ray scattering supports presence of heme-bound dimer of SbMSBP1

Next, we used small angle X-ray scattering (SAXS) to better understand the structure of the heme-bound oligomeric form of SbMSBP1$^{\Delta N}$. Dimensionless Kratky plots for both apo- and heme-SbMSBP1$^{\Delta N}$ indicate a mixture of folded and disordered regions, consistent with disorder of the C-terminus (Fig. 2c). Plots for lower protein concentrations show less distinct bell-shaped features at $q/R_g = 3$, relative to the rising signal at increasing q/R_g (Supplementary File 1), suggesting higher flexibility at lower concentrations. Approximated R_g-values were larger for heme-SbMSBP1$^{\Delta N}$ than apo-SbMSBP1$^{\Delta N}$, (34.18 ± 1.02 Å and 28.15 ± 0.66 Å, respectively, Supplementary File 1), but the high degree of flexibility precluded molecular weight estimation and maximal particle dimensions (D_{max}) estimation from pair-distance distribution functions.

We next used ensemble optimization method (EOM) to model scattering profiles (Kikhney and Svergun 2015, Tria et al. 2015). We used the AlphaFold2 structure of SbMSBP1$^{\Delta N}$ (Jumper et al. 2021), and treated the cytochrome b_5-like domain of SbMSBP1 as a rigid body and N- and C-terminal regions (residues 45–65 and 169–223, respectively) as disordered, which is consistent with our data shown above and with low predicted Local Distance Difference Test (pLDDT) scores (<70) for these regions in the AlphaFold2 model. We then generated combined pools consisting of 10 000 models each in monomer and dimer conformations (based on the dimer structure of human PGRMC1). EOM ensembles showed good fits to the experimental scattering profiles for both

apo- and heme-SbMSBP1$^{\Delta N}$ proteins at all concentrations (Fig. 2d, Supplementary File 1). The R_g and D_{max} distributions of the selected model ensembles at 5 mg mL^{-1} showed one and two major peaks for apo-SbMSBP 1$^{\Delta N}$ and heme-SbMSBP1$^{\Delta N}$, respectively (Fig. 2e and f), and R_g estimates at all concentrations showed good agreement with Guinier estimates (Supplementary File 1). Inspecting the models in the ensembles selected by EOM, apo-SbMSBP1$^{\Delta N}$ ensembles exclusively comprise monomers, except at the highest concentration, whereas the heme-SbMSBP1$^{\Delta N}$ ensembles comprise a mixture of monomers and dimers at all concentrations (Supplementary File 1). Together, our data shows that heme binding induces a shift towards a higher order oligomeric state consistent with a dimeric conformation.

SbMSBP1 expression is correlated with SNARE proteins in *S. bicolor* and is distinct from other MSBP isoforms

In barley (*Hordeum vulgare*), the closest *SbMSBP1* homolog (*HvMSBP1*) has been shown to be highly upregulated in response to salt stress and knockout of the *Arabidopsis* homolog *AtMSBP1* showed altered root morphology that could be rescued by expression of the barley protein (Witzel et al. 2018). Together, these lines of evidence indicate that these proteins could have wide-ranging functions across many tissues. We sought to investigate whether this characteristic is shared with sorghum MSBP proteins and uncover proteins with similar patterns of expression by growing *S. bicolor* seedlings in water or 100 mM NaCl for 7 days before dissecting into root, stem (mesocotyl), and tip and performing tissue-level global proteomics (Fig. 3a). We could quantify a total of 11 312 protein groups for the entire dataset with median coefficients of variation below 13% (Supplementary File 1). After normalization and imputation (Supplementary File 1), we observed clear separation according to tissue type along the first and second principal component axes, and separation according to treatment along first and third principal component axis (Fig. 3b and c). A total of 2799 proteins were significantly different in salt-treated samples across all tissues ($P > 0.001$, Supplementary File 1).

Terms for response to chemical and salt stress were among the significantly upregulated proteins in all tissues, confirming the effect of the treatment applied, with other stress-response and signaling-related terms showing more tissue-specific enrichment, such as oxylipin biosynthesis and gluthathione-related processes (Supplementary File 1), while processes related to central metabolism and photosynthesis were enriched among downregulated proteins (Supplementary File 1). Altogether, our enrichment analysis finds systemic responses consistent with the applied salt treatment. To compare the abundances of individual *S. bicolor* MAPR proteins, we compared intensity-based absolute quantities (iBAQ), which summarize protein abundances to provide intensities equivalent to molar concentrations (Schwanhausser et al. 2011). Based on iBAQ intensities, SbMAPR2 was the most abundant MSBP homolog, consistently in the top 95th percentile of proteins, while SbMSBP1 was the second most abundant homolog across tissues and treatments (Supplementary File 1). SbMSBP4 was the third most abundant homolog, except in tips, where SbMSBP3 abundance was comparable (Supplementary File 1). To investigate proteins with related patterns of accumulation to SbMSBP1 in our dataset (Fig. 3d), we performed weighted gene co-expression network analysis (WGCNA), which yielded 26 distinct clusters (Supplementary File 1). The *S. bicolor* MAPR proteins were grouped into five clusters and SbMSBP1 alone fell into cluster darkturquoise, which comprised proteins increasing in abundance in response to salt treatment across all tissues (Fig. 3e). Gene ontology (GO) enrichment analysis of the darkturquoise cluster found enrichment of proteins related to SNARE-dependent ER-Golgi vesicle transport (Fig. 3f). Our proteomics data thus implicate SbMSBP1 in vesicle-mediated transport between these endomembrane compartments.

SbMSBP1 expression induces formation of ER-derived vesicles in protoplasts and tobacco: effect appears to be independent of heme-binding

To investigate the functional role of SbMSBP1 in vesicle-mediated transport, we expressed SbMSBP1 fused to monomeric enhanced green fluorescent protein (mEGFP) in protoplasts derived from 6-day-old *S. bicolor* seedlings and examined its localization by confocal laser scanning microscopy. Expression of SbMSBP1-mEGFP led to the formation of what appeared to be thick-walled vesicles and to a lesser extent strands reminiscent of ER membrane (Fig. 4a, left). To investigate whether these structures could be ER-derived, we co-expressed theSbMSBP1-mEGFP fusion protein with an ER membrane marker (Fig. 4a, middle) derived from the N-terminal ER membrane anchor of *Arabidopsis* CYP51G1 (Bassard et al. 2012), as well as a soluble fluorophore targeted to the ER lumen (Fig. 4a, right) by fusion with rice α-amylase 8 and an ER retention signal (SEKDEL). In both cases, we observed similar vesicles upon co-expression of ER markers with SbMSBP1-mEGFP, with overlapping signals for both fluorophores. We generally saw low expression of the luminal ER marker when co-expressed with soluble mEGFP, but much stronger signal in the presence of SbMSBP1, which may derive from concentration of marker signal in these membrane vesicles. The vesicles show increased membrane thickness reminiscent of that previously reported for whorls of organized smooth ER (OSER) (Agee et al. 2010, Ferrero et al. 2015, Sandor et al. 2021), or possibly vacuolar bulbs (Saito et al. 2011, Segami et al. 2014), and z-stacks suggest these structures form elongated vesicles in the cell (Supplementary Files 4-6). To ensure the observed vesicles were not due to overexpression driven by the 35S promoter, we also expressed SbMSBP1-mEGFP under control of its own promoter comprising 1.6 kb upstream of the SbMSBP1 start codon (Fig. 4b). In this case, we still observed the formation of vesicles, though they were lower in number and generally smaller in size than observed in the case of 35S expression, suggesting vesicle formation

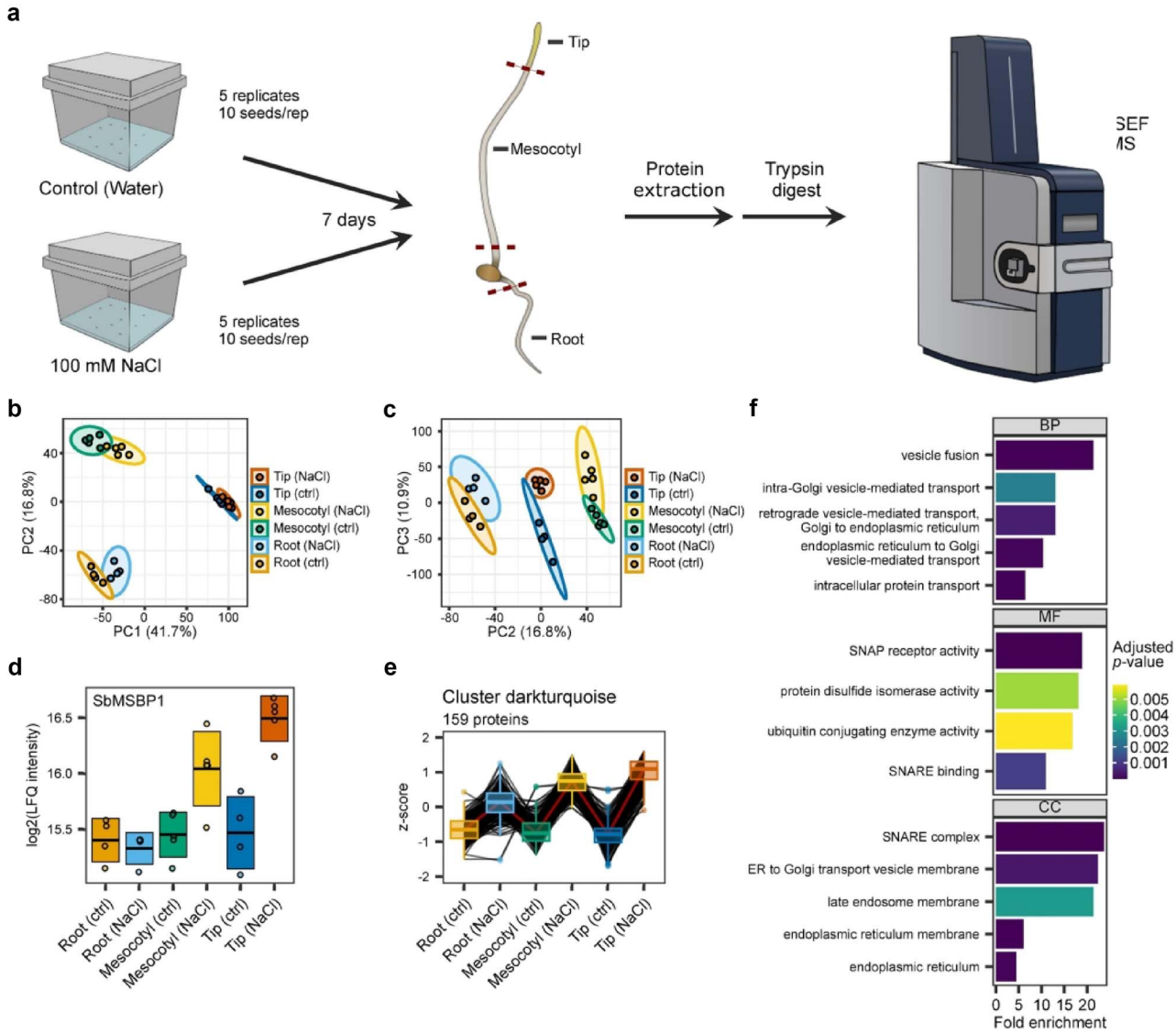

Figure 3. Untargeted proteomics of roots, stem (mesocotyl), and tip from sorghum seedlings under salt stress. (a) Outline of the salt stress experiment. (b) Principal component analysis of label-free protein quantities in treated and control tissue samples shows clear separation according to tissue types along first and second principal components (PC). (c) Principal component analysis showing PC2 and 3, with separation along PC3 according to treatment. (d) Label-free quantities of SbMSBP1. Centerline of boxes indicate mean LFQ intensities, with box edges indicating one standard deviation. (e) Scaled expression profile for proteins belonging to WGCNA cluster darkturquoise. Means of scaled LFQ intensities of individual proteins are plotted as black lines, while the cluster median is indicated by a red line. Overlaid boxplots show data distribution for individual proteins in each condition. (F) GO enrichment of proteins belonging to the darkturquoise cluster. BP, biological process; MF, molecular function; CC, cellular compartment.

and morphology is to an extent dose dependent. We next investigated the origin of these vesicles by co-expressing them with organellar markers for Golgi, plasma membranes, and peroxisomes (Fig. 4c). We observed some overlap between the SbMSBP1-mEGFP signal and the Golgi marker, suggesting the vesicles may arise from ER-to-Golgi membrane trafficking (Fig. 4c, left). We observed no overlap between the signal for plasma membrane or peroxisomes (Fig. 4c, middle and right). Neither did structures labeled by the plasma membrane marker resembling endosomes overlap with the SbMSBP1-mEGFP signal, in contrast with reports showing the endosome-derived vesicles formed by overexpression of *Arabidopsis* MSBP1 (Song et al. 2009). Attempts to express known vacuolar markers (Nelson et al. 2007, Han et al. 2022) in sorghum protoplasts were not successful. Truncation of the C-terminal disordered domain of SbMSBP1 did not attenuate vesicle formation (Fig. 4d, left panel). Since similar ER-derived structures have been shown to form by expression of the TM domains of different ER-localized proteins (Ferrero et al. 2015, Sandor et al. 2024), we also tested the ability of the N-terminal TM domain (residues 1–44) of SbMSBP1 to cause formation of ER-derived vesicles. We still observed some vesicle formation

in protoplasts with just the TM domain, though it appeared less prevalent, while expression appeared more punctate than vesicular in tobacco, suggesting the TM domain alone is not sufficient for the formation of large thick-walled vesicles observed (Fig. 4d, right). In addition to sorghum protoplasts, we also observed the formation of vesicle structures when expressing SbMSBP1 variants transiently in tobacco, though the structures were smaller and less prominent, suggesting species specific interactions with other cellular machinery may be involved (Supplementary File 1). Together, these results suggest that SbMSBP1 plays a role in the formation of OSER structures, which is consistent with the correlation observed with vesicle trafficking processes in our proteomics data (Fig. 3).

Discussion

MAPR phylogeny reveals clades distinct to the plant and animal lineages

Sorghum encodes six MAPR proteins according to the Panther classification system (Fig. 1a). To our knowledge, this study is the first systematic investigation reported for plant MAPR subclasses. Although MAPR isoforms in sorghum appear superficially similar, more in-depth investigation reveals that only proteins in the MSBP clade are likely to possess TM anchors (Fig. 1b). In contrast, proteins in the plant NEUFC clade appear instead to contain N-terminal signaling peptides, possibly directing these proteins for secretion as reported for animal NEUFCs (Kimura et al. 2010b). The phylogeny reported here suggests that the NEUFC family predates the split between animals and plants, but the relatively close clustering of the clades suggests that they remain under selective pressure. Though the *Arabidopsis* NEUFC has been found to be induced by auxin-like signals during nematode infection in *Arabidopsis* (Cabrera et al. 2014), there is very little known about the functions of these proteins in plants. The c-cup clade appears to be a plant-specific clade that comprises just a cytochrome b_5-like domain (Fig. 1a and b). The *Arabidopsis* member of this clade, AtMAPR2, has been structurally characterized by NMR to harbor a fold very similar to the cytochrome b_5-like domains of other MAPR proteins (Song et al. 2004). Though they lack TM domains, the AtMAPR2 was found to be associated with the membrane proteome in plants lacking key enzymes of glucosinolate biosynthesis (Mostafa et al. 2017). Somewhat conflictingly, AtMAPR2 was also found in apoplast fractions of *Arabidopsis* plants subjected to pathogen stress (Strehmel et al. 2017), and just like the NEUFCs, the functions of MAPR proteins belonging to the c-cup clade are generally poorly understood.

Dynamic heme dependent dimerization of sorghum MSBP1 and functional implications

Here, we combine multiple biophysical methods to demonstrate that SbMSBP1 binds to ferric heme and that heme binding results in dimerization (Fig. 2, Supplementary File 1). The functional consequence of the preference of SbMSBP1 for oxidized heme remains unclear; however, it further supports that SbMSBP1 is not involved in electron transfer processes. The heme binding ability seems to be a shared feature of the MAPR family, which may support the proposal that the protein plays a role in heme metabolism by functioning as a heme chaperone, as demonstrated for human PGRMC1 and PGRMC2 (Galmozzi et al. 2019). It is important to note that SbMSBP1 existed in an equilibrium between a heme bound and apo configuration during the expression and purification in *Escherichia coli* (Supplementary File 1), although the heme precursor δ-ALA was supplied during protein production. This suggests that the heme-binding of MSBP may be reversible. The functional implications of heme-dependent dimerization remain elusive, as we cannot presently determine whether the protein occurs as heme-bound dimer in vivo. Phosphorylation has been proposed to occur on heme-coordinating Y113 of human PGRMC1, though it remains to be experimentally verified (Cahill et al. 2016). This would provide a mechanism to regulate heme-dependent dimerization and would suggest that heme-dependent dimerization serves a real biological role.

Is SbMSBP1 a steroid-binding protein?

Progesterone binding was originally associated with PGRMC1 based on binding assays using partially purified fractions from porcine liver (Meyer et al. 1996), and later confirmed on purified proteins by UV–Vis and resonance Raman (Kaluka et al. 2015). Likewise, *A. thaliana* MSBP1 was shown to bind progesterone as well as a number of plant-specific steroids, including BRs and stigmasterol (Yang et al. 2005). In our study using purified apo-SbMSBP1, we could not observe direct progesterone binding (Supplementary File 1). It is possible that the removal of the N-terminal TM anchor in our experiments prevented binding, although previous data from PGRMC1 indicate the site of progesterone binding to be proximal to the heme-binding pocket (Kaluka et al. 2015). Alternatively, progesterone binding may be specific to the heme-bound protein, as shown to be the case for analogs of the steroid-like triterpene glycyrrhizin binding to PGRMC1 (Kabe et al. 2021), although this contradicts available evidence for progesterone binding by PGRMC1 (Kaluka et al. 2015). A third possibility is that SbMSBP1 may not bind progesterone but show strict substrate specificity toward plant sterols. Although this contradicts findings that AtMSBP1 has the highest affinity toward progesterone (Yang et al. 2005), we cannot currently exclude either explanation, and steroid binding for the sorghum protein needs to be further studied.

SbMSBP1 may induce formation of organized smooth endoplasmic reticulum

Here, we show by fluorescence-based confocal microscopy that SbMSBP1 localizes to the ER membrane, consistent with previous reports on different MAPRs (Kuhn et al. 2010, McGuire et al. 2021), and that SbMSBP1 expression promotes the formation of ER-derived vesicles independently of the C-terminal disordered domain (Fig. 4). These results are consistent with our proteomics data, which implicate SbMSBP1 in vesicular trafficking and re-location between membranous

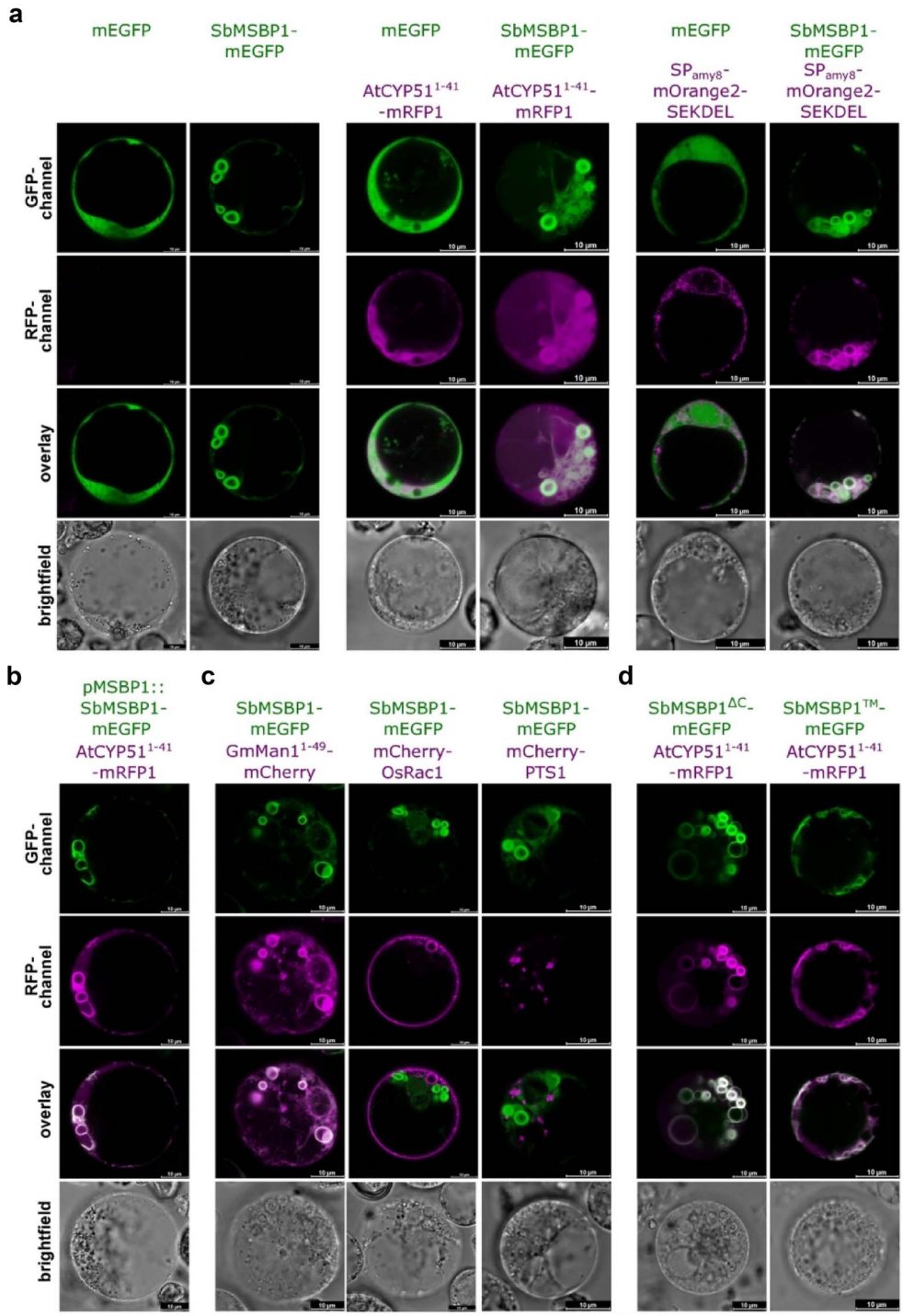

Figure 4. Changes in ER membrane morphology upon expression of SbMSBP1 in sorghum protoplasts. Confocal microscopy showing sorghum protoplasts transiently transformed with SbMSBP1 constructs fused to mEGFP (GFP-channel), co-transformed organellar markers. (a) Expression of free mEGFP and SbMSBP1-mEGFP alone or in conjunction with the ER membrane marker AtCYP51$^{1-41}$-mRFP1 or the ER luminal marker SP$_{amy8}$-mOrange2-SEKDEL. (b) expression of SbMSBP1-mEGFP under control of its native promoter (pMSBP1). (c) Expression of SbMSBP1-mEGFP in combination with markers for Golgi (GmMan1$^{1-49}$-mCherry), plasma membrane (mCherry-OsRac1), or peroxisomes (mCherry-PTS1). (d) Expression of truncated SbMSBP1 variants in combination with the ER membrane marker AtCYP$^{1-41}$-mRFP1. SbMSBP$^{\Delta C}$-mEGFP comprises the core protein without its unstructured C-terminal domain (residues 1–174). SbMSBP™-mEGFP comprises the N-terminal transmembrane anchor domain (residues 1–44). Expression for all constructs was driven by the CaMV 35S promoter unless otherwise stated. Scale bars correspond to 10 μm in all images.

subcellular compartments under cellular adaptations to stress conditions (Fig. 3). In contrast, with the reported localization of *Arabidopsis* MSBP1 plasma membrane and endosomes (Song et al. 2009), we could not observe co-localization of SbMSBP1 with plasma membrane or associated endosomes (Fig. 4c), which suggests functional divergence even among proteins with relatively close evolutionary relationship. Despite this, our data are broadly in agreement with reports of MSBP1 interactions with overexpressed SNARE protein in plasma membrane fractions of *A. thaliana* (Zhu et al. 2014), and are consistent with the finding that the barley MSBP1 homolog shows higher abundance in salt tolerant cultivars (Witzel et al. 2018). Several studies have shown that MAPR proteins stabilize enzymes of the cytochrome P450 family (Rohe et al. 2009, McGuire et al. 2021) including the widespread sterol 14α-demethylase (CYP51) that catalyzes a critical step in sterol biosynthesis. At the same time, the implication of AtMSBP1 as a negative regulator of BR signaling, possibly via a SNARE-dependent mechanism (Song et al. 2009, Zhu et al. 2014), may suggest a link between sterol biosynthesis and vesicle trafficking, including a functional role in sterol deposition to the plasma membrane in response to abiotic stresses such as salinity.

Vesicles formed upon expression of GFP-tagged SbMSBP1 variants showed a distinct, thick-walled morphology that was similar to that reported for a phenomenon known as OSER (Korkhov and Zuber 2009, Agee et al. 2010, Sandor et al. 2021). Vacuolar bulbs with similar morphology were also reported in *Arabidopsis* and found to originate from vacuolar membranes (Saito et al. 2011, Segami et al. 2014). Although we were not able to find a functioning tonoplast marker, which means we cannot completely exclude vacuolar involvement in the structures observed, strong overlap with ER and Golgi membranes (Fig. 4a and c) suggest that OSER-like structures may be a more likely explanation. OSER has been primarily studied and implicated in ER stress responses in animal cells, though several plant proteins have been implicated in OSER formation as well (Korkhov and Zuber 2009, Ferrero et al. 2015, Sandor et al. 2021, Sandor et al. 2024). OSER is reported to occur both as crystalline membranous arrays, as well as multilamellar whorls based on electron microscopy (Ferrero et al. 2015); however, the vesicles observed in our study generally only resemble whorls (Fig. 4), whose multilamellar organization may explain the apparent increased membrane thickness of these vesicles. Recently, proteins that induce OSER formation and its associated ER membrane proliferation have been proposed as a tool for metabolic engineering by compartmentalizing and scaffolding of biosynthetic enzymes (Sandor et al. 2021), and this idea is supported by studies showing that membrane anchoring facilitates assembly of dynamic metabolome complexes (Laursen et al. 2021). In this context, and given reports of cytochrome P450 stabilization by MSBP proteins (Rohe et al. 2009, McGuire et al. 2021), our data suggest that SbMSBP1 could serve as an addition to this particular metabolic engineering toolset, though its applicability in this context remains to be demonstrated.

Conclusions

Identification and characterization of key proteins involved in stress resilience is critical for the development of our future crops. Here, we combine biochemical approaches with structural biology, proteomics, bioinformatics, and microscopy to provide a characterization of one of the key "mysterious" proteins involved in salt tolerance and plant metabolism. In accordance with its orthologue protein in human cells, PGRMC1, SbMSBP1 is capable of forming a homo-dimer in a heme-dependent manner. To our knowledge, the present study is the first report on this ability of the MAPR family from plant species. In addition, the protein contains an extended flexible region at the C-terminus. In our studies, the C-terminal region does not seem to be required to induce vesicle formation but may instead be involved in signaling or regulation of vesicle formation in a yet unknown capacity. The finding that MSBP1 from sorghum is involved in ER-derived vesicle transport provides the foundation for future studies on plant engineering for improved salt tolerance, and may provide a useful tool for ER membrane compartmentalization of engineered biosynthetic pathways.

Materials and Methods

Phylogenetic analysis

All sequences belonging to the Panther family PTHR10281 (Membrane-Associated Progesterone Receptor Component-Related, 526 sequences) were downloaded from https://pantherdb.org (Thomas et al. 2022). Sequences were aligned using MAFFT (Lemoine et al. 2019). Alignments were manually inspected and subsequently trimmed using ClipKIT (Steenwyk et al. 2020). Phylogenetic trees were constructed using the IQ-TREE web server (Trifinopoulos et al. 2016) with automatic substitution model prediction and 1000 iterations of ultrafast bootstrapping. Trees were annotated using Interactive Tree Of Life (accessed at itol.embl.de).

Molecular cloning and plasmid constructions

The cDNA encoding different *S. bicolor* MSBP constructs, SbMSBP1$^{\Delta N}$ (a.a.45–223), SbMSBP1$^{\Delta N,C}$ (a.a. 45–174) and SbMSBP1^{C} (a.a.175–223), were prepared by PCR using the cDNA of full-length protein as a template and included an N-terminal TEV site just upstream of the first amino acid of each protein variant. All gene constructs were inserted into pET28c+ using NdeI and XhoI sites to retain the N-terminal 6xHis-tag and thrombin site but omit the T7 tag encoded by the vector. A stop codon was included in the insert to avoid the 6xHis-tag encoded by the vector. All gene constructs were confirmed by DNA sequencing (Marcogen). For expression in protoplast, a pUC57 vector was constructed with either a native SbMSBP1 promoter or the 35S constitutive promoter from Cauliflower mosaic virus (CaMV) and different SbMSBP1 variants, fused to mEGFP. For the native promoter construct, 1.6 kb upstream of the start of transcription of SbMSBP1 was amplified from *S. bicolor* genomic DNA (isolated from leaf tissue of *S. bicolor* seedlings using the QIAGEN DNeasy Plant Kit). For expression in tobacco, the corresponding constructs were assembled in the vector pK2GW7 (Karimi et al. 2002). USER cloning was used to assemble the plasmids. Construction of the ER control comprising the N-terminal 41 residues of *A. thaliana* CYP51 fused to mRFP was previously described (Bassard et al. 2012). An ER lumen control adapted from Wu et al. (2016) was made by fusing the N-terminal targeting sequence of rice α-amylase 8 sequence and the C-terminal ER retention signal to mOrange2 under the control of the maize ubiquitin promoter. Organellar markers for Golgi and peroxisomes from

(Nelson et al. 2007) were used as binary vector constructs. The rice plasma membrane marker pUC19/mChe-PM (Han et al. 2022) was a gift from Yao-Guang Liu and Qinlong Zhu (Addgene plasmid # 183168; http://n2t.net/addgene:183168; RRID:Addgene_183 168).

Protein expression

The pET28c+ vector harboring genes encoding different protein constructs were transformed into *E. coli* strain NiCoBL21(DE3). A starter culture was grown overnight at 37 °C with a shaking of 220 rpm in lysogeny broth containing kanamycin (50 μg mL^{-1}). The overnight culture was then transferred into a fresh terrific broth medium supplemented with kanamycin (50 μg mL^{-1}) with a ratio of 1:10 and incubated at 37 °C at 180 rpm until an OD600 ~1.5–2. The cells were induced by adding isopropyl 1-thio-β-D galactopyranoside to the final concentration of 250 μM. The heme precursor, δ-aminolevulinic acid, was also added to the final concentration of 0.5 mM during induction. The culture was then continued overnight at 25 °C at 180 rpm. ^{15}N-labeled protein was prepared as above but cells were grown in minimal M9 media prepared with $^{15}NH_4Cl$ as N-source and containing kanamycin (50 μg mL^{-1}).

Protein purification of TM truncated MSBP constructs

Overnight cultures expressing labeled and unlabeled proteins were harvested and cells were disrupted using a benchtop cell disruptor (Constant Systems Ltd, Northants, UK). Crude extracts were centrifuged at 15 000 *g* for 45 min at 4 °C. The supernatant was collected and filtered through a syringe filter with a pore size of 0.45 μm. TM truncated SbMSBP1 constructs were purified using two chromatographic steps. First, the crude extracts were passed through HisTrap HP prepacked column equilibrated with the binding buffer (1× PBS pH 7.4). The column was then washed 6 column volumes (CV) using 10% elution buffer (1× PBS pH 7.4 containing 500 mM imidazole). Bound proteins were eluted with a linear gradient (10%–100%) within 6 CV. In the second purification step, samples from the first step were first subjected to buffer exchange. The samples were loaded to Q-Sepharose High-Performance prepacked column equilibrated with 20 mM sodium phosphate buffer pH 6.5. The bound protein was eluted with a linear gradient of 1%–70% within 10 CV and followed by a step gradient of 100% with elution buffer (20 mM sodium phosphate buffer pH 6.5 containing 1 M NaCl). The purified fractions were collected, and the purity was judged by SDS-PAGE. The fractions were pooled and kept on ice or at −70 °C for further steps.

HISx6 tag removal

The Hisx6 tag in TM truncated SbMSBP1 constructs was removed using in-house TEV protease. The cleavage reaction was done in TEV protease buffer (50 mM Tris–HCl pH 8.0). A 25:1 ratio of purified protein:protease was used, and the reaction was done at 4 °C overnight. The non-tagged protein was separated using inversed IMAC. The flow-through was collected and concentrated before applying it to SEC.

Analytical size exclusion chromatography

The protein–heme interaction was investigated using an apo SbMSBP1 fraction. The protein concentration was kept constant at 50 μM. The mixture of different protein:hemin ratios were prepared (1:0.1, 1:0.5, 1:1, and 1:2). The effect of heme binding was observed using analytical SEC connected to Shimadzu HPLC system coupled with a diode array detector. The 100 μL samples were injected onto Superdex 200 Increase 10/300 GL column equilibrated with a running buffer of 50 mM sodium phosphate pH 7.0 containing 150 mM NaCl. The flow rate was kept constant at 0.5 mL min^{-1}. The elution profiles of the heme-bound proteins were followed at 280 and 400 nm.

NMR spectroscopy

All samples were dialyzed into buffer containing 50 mM phosphate (pH 7.0) and 150 mM NaCl containing 10% D_2O and 250 μM 4,4 dimethyl-4-silapentane-1-sulfonic acid as internal standard. 2D ^{1}H-^{15}N-HSQC spectra were recorded at 50 and 500 μM protein concentrations. A protein concentration of 50 μM was used for heme and progesterone interaction studies. All NMR experiments were conducted using a Bruker Ascend 800 MHz spectrometer available at cOpenNMR, Department of Biology, University of Copenhagen. Bruker TopSpin 3.5 software was used to control the spectrometer and process the spectra. Further analysis and final figures are made using Collaborative Computational Project for NMR (CCPN) (Skinner et al. 2016).

Small-angle X-ray scattering

Prior to analysis by SAXS, apo- and heme-bound proteins were dialyzed against the buffer containing 50 mM sodium phosphate (pH 7.0) and 150 mM NaCl at 4 °C overnight. For each protein, four different concentrations were prepared (1.25, 2.5, 5, and 10 mg mL^{-1}). Samples were centrifuged at 15 000 rpm for 20 min before being loaded on a sample plate kept at 10 °C during the experiment. SAXS studies were performed at the CPHSAXS Facility, University of Copenhagen, on a Xenocs© BioXolver L with a wavelength (λ) of 1.34 Å. The detector distance of 632.5 mm corresponding to the q range of 0.015–0.5 Å-1 was used. Scattering data were collected at 25 °C for 40 frames with an exposure time of 60 s per frame for protein samples and the corresponding buffer. Buffer scattering was subtracted from averaged protein scattering profiles. Primary data reduction and analysis were made in BioXTAS RAW (Hopkins et al. 2017).

Ensemble optimization method

A model was created from the SbMSBP1 amino acid sequence using AlphaFold2 (Jumper et al. 2021) on the Google ColabFold server (Mirdita et al. 2022). The amino acid cut-off for the core structure of SbMSBP1 was found by comparing it to the structure of human PGRMC1 (PDB id: 4X8Y). The model of SbMSBP1 monomer was used to create a dimer in PyMOL (Version 2.1 Schrödinger, LLC) by superimposing the heme stacking dimer in a crystal structure of the human PGRMC1. The selection of core structure and flexible segments obtained in this step were then used as inputs to RANCH using ATSAS 3.2.1 (Manalastas-Cantos et al. 2021). Briefly, a pool of PDB models of monomer (10 000 models) and dimer (10 000 models) was generated by RANCH. FFMAKER was run on combined pools of monomers and dimers to calculate scattering intensities and R_g of models. The genetic algorithm GAJOE was then applied for the optimal selection of structures resembling experimental scattering data.

Plant material and protein extraction for global proteomics

Seeds of *S. bicolor* (L.) Moench *cv* BTx623, washed in tap water, were pre-germinated in tap water for 16 h at 28 °C in the dark and grown on filter paper soaked with 20 mL tap water or 20 mL tap water containing 100 mM NaCl for 5 days at 28 °C in darkness. Five biological replicate pools of 20 seedlings were used per condition. Seedlings were divided into root, mesocotyl, and tip, frozen in liquid N_2 and ground using a mortar and pestle cooled with liquid N_2. Protein extraction was done by adapting a modified TCA:acetone protocol (Niu et al. 2018) as follows: Protein was extracted from 100 mg ground tissue with six volumes protein extraction buffer (4% SDS, 100 mM tris pH 8.2, 500 mM NaCl, 10 mM DTT) supplemented with complete EDTA-free protease inhibitors (Roche) with brief boiling (95 °C, 3 min) followed by centrifugation. The pellet was re-extracted with the same buffer and the clarified extracts combined. Protein was precipitated by adding an equal volume 20% TCA in acetone (supplemented with 5 mM DTT) and incubating 1 h at −20 °C. Precipitate was recovered by centrifugation (15 000 *g*, 3 min) and the resulting pellet washed once in 100% acetone and three times in 80% acetone (with 1 mM DTT). Protein pellets were resuspended in EasyPep Lysis buffer (Thermo Scientific) with 3 μL

Universal Nuclease (25 kU) and homogenized using a BeatBox homogenizer (Preomics) at high setting for 10 min. Protein concentration was measured after centrifugation using BCA assay (Pierce) and 50 μg protein reduced with 5 mM tris(2-carboxyethyl)phosphine for 15 min at 55 °C before alkylation with 20 mM 2-chloroacetamide for 30 min at RT. Protein was digested using 1:50 (μg:μg) Trypsin/LysC (Promega) for 16 h at 37 °C. Peptide cleanup was performed using a Peptide Clean-Up Plate (Thermo Scientific).

Global proteomics data acquisition

Peptides (200 ng) were injected on an Aurora Gen2 C18 column (250 × 0.075 mm, 1.6 μm, IonOpticks, Melbourne, Australia) using a Vanquish Neo UHPLC (Thermo Scientific). Peptides were separated using a 90 min gradient as follows: 2%–17% B (0.1% formic acid in acetonitrile) over 56 min; 17%–25% B over 21; 25%–35% B for 13 min. A flow rate of 400 nL min^{-1} was used, and column temperature was kept at 50 °C. The column was connected via a CaptiveSpray source with a 20 μm emitter to a timsTOF Pro 2 mass spectrometer (Bruker, Bremen, Germany), which was operated in diaPASEF mode. MS data acquisition was performed over a 100–1700 m/z range with a PASEF cycle time of 1.8 s. Each acquisition cycle used 16 diaPASEF scans with two 25 Da windows per ramp (100 ms accumulation and ramp time) over 400–1201 m/z mass range and 1.43–0.6 Vs cm^{-2} mobility range. Collision energy was decreased linearly from 59 eV at 1.6 Vs cm^{-2} to 20 eV at 0.61 Vs cm^{-2}. Ion mobility calibration was performed using Agilent ESI-L Tuning Mix.

Data processing

Proteomics data were processed using DIA-NN v1.8.1 (Demichev et al. 2020, Demichev et al. 2022) in library-free mode against the *S. bicolor* proteome from Uniprot (UP000000768) and the universal proteomics contaminants list (Frankenfield et al. 2022). Search settings were: Protease set to Trypsin/P, maximum 1 missed cleavage, N-terminal Met excision and Cys carbamidomethylation enabled, Met oxidation as variable modification (max 3 variable modifications allowed). Only peptides of 7–42 residues with a 1–4 charge state were considered, in a 300–1800 precursor m/z range and a 200–1800 m/z fragment ion range. Precursor false discovery rate was set to 0.01. Match between runs was enabled, with heuristic inference and no shared spectra enabled. Protein inference was set at genes, and quantification done using robust LC (high precision) mode, with RT-dependent cross-run normalization and smart profiling library generation. The mass spectrometry proteomics data have been deposited to the ProteomeXchange Consortium via the PRIDE (Perez-Riverol et al. 2022) partner repository with the dataset identifier PXD058939.

Proteomics data analysis

Label-free quantity (LFQ) and iBAQ were calculated in R using DIAgui (Gerault et al. 2024). Subsequent analysis was performed in R using functions from the packages DEP (Zhang et al. 2018), clusterprofiler (Yu et al. 2012) and WGNCA (Langfelder and Horvath 2008), along with in-house scripts. For both LFQ and iBAQ, data were filtered to remove contaminants and proteins without at least four valid values in one group. Three samples were discarded due to low number of protein identifications. Data were normalized by variance stabilizing normalization and LFQ data imputed with mixed imputation (kNN for MAR and QRILC for MNAR). For iBAQ, data were used after normalization without imputation. Group comparisons was performed using DEPs implementation of limma (Ritchie et al. 2015), followed by Benjamini–Hochberg FDR correction (Benjamini and Hochberg 1995). Weighted gene co-expression network analysis was performed using log-transformed LFQ values after normalization and mixed imputation. A soft threshold β of 14, signed hybrid and biweight midcorrelation were used to calculate network adjacency, and generate signed topological overlap. Module identification was done using a minimum module size of 30, and modules with correlation greater than 0.9 were merged. GO enrichment was performed using Benjamini–Hochberg FDR correction and an adjusted *P*-value cut-off of 0.05.

Protoplast isolation and transformation

Sterilized seeds of *S. bicolor* (L.) Moench *cv* BTx623 were incubated in water for 1 h and placed in cell culture boxes containing 2.2 g L^{-1} Murashige & Skoog medium including vitamins (Duchefa), and 8.5 g L^{-1} Micro agar (Duchefa). Seedlings were grown in the dark for 6 days at 28 °C. Between 1.5 and 2 g of etiolated hypocotyl tissue was cut into 1–2 mm thin pieces in 10 mL of mannitol buffer (600 mM D-mannitol, 2 mM MES, pH 5.7). Mannitol buffer was subsequently replaced by 10 mL of digestion buffer (600 mM D-mannitol, 10 mM MES, 7.5 mM $CaCl_2$, pH 5.7) containing 1.5% macerozyme R10 (Duchefa), 1.5% cellulase R10 (Duchefa), 0.1% bovine serum albumin (BSA), 0.1% Polyvinylpyrrolidone (PVP40) and incubated for 3–4 h at 25–28 °C in darkness. Then, 10 mL of W5 buffer (154 mM NaCl, 125 mM $CaCl_2$, 5 mM KCl, 2 mM MES, pH 5.7) was added with gentle mixing and the mixture strained via a 40–70 μm cell strainer before diluting with equal volumes W5 buffer. Suspensions were centrifuged for 20 min at 100 *g* in a swing-out rotor centrifuge with the brake disengaged. The pellet was washed with 30 mL of W5 buffer and centrifuged for 10 min. Cell density was determined using a Fuchs-Rosenthal Counting Chamber with a cell-depth of 0.2 mm of pellets resuspended in 15 mL of W5 buffer. Finally, cells were pelleted and resuspended in MMG solution (400 mM D-mannitol, 100 mM $MgCl_2$, 4 mM MES, 5 mM $CaCl_2$, pH 5.7) to a concentration of 2000 protoplasts μL^{-1}. Protoplasts were incubated for 5 min at 45 °C and immediately placed on ice for 1 min before transforming by adding 7.5 μg of purified plasmid DNA for 200 μL protoplast suspension to each tube with gentle mixing. Next, 200 μL of PEG solution (40% w/v polyethylene glycol 4000, 200 mM *D*-mannitol, 100 mM $CaCl_2$) was added and gently mixed before incubating for 20 min in the dark. Afterward, 900 μL of W5 solution was added followed by centrifugation at 130 *g* for 7 min. Pellets were resuspended in 500 μL of W5 solution and suspensions were incubated at 28 °C in the dark for 15–24 h.

Transient expression in tobacco

Four-week-old *N. benthamiana* plants were used to infiltrate a combination of *Agrobacterium* GV3101 strains carrying (i) different variants of SbMSBP1 fused to mEGFP, (ii) an ER-membrane marker (Bassard et al. 2012), comprising the N-terminal 41 residues of *Arabidopsis* CYP51G1 (Uniprot accession Q9SAA9), together with empty pEAQ-HT supplying the p19 suppressor of silencing gene. *Agrobacterium* strains were suspended in 10 mM MES, 10 mM $MgCl_2$, 200 μM acetosyringone to a final OD of 0.5 per strain before infiltrating in the abaxial side of the leaf using a needleless syringe. Plants were maintained under greenhouse conditions for 3 days before confocal microscopy.

Confocal laser scanning microscopy

Protoplasts were loaded on an 18-well μ-slide (ibidi) pre-treated with 0.1% w:v poly-L-lysine (Sigma-Aldrich) and left to deposit for a few minutes. Tobacco leaf discs were mounted in water on a standard microscopy slide. Then the samples were imaged on a STELLARIS 8 (Leica Microsystems) laser-scanning confocal microscope using a 40× glycerol-immersion objective (Leica Microsystems Type G Immersion Liquid). All fluorescent channels were acquired sequentially, (489 nm/499–538 nm excitation/emission for mEGFP,590 nm/600–649 nm ex./em. for mRFP1, 548 nm/558–598 nm ex./em. for mOrange2 and 587 nm/597–630 nm ex./em. for mCherry). The images were analyzed with Leica Application Suite X Office. The intensity of the signal for each channel was adjusted post-processing to compensate for difference in signal intensity between red and green channels.

Acknowledgments

We acknowledge the University of Copenhagen, Small angle X-ray facility, CPHSAXS, funded by the Novo Nordisk Foundation (grant no. NNF19OC0055857). NMR data were recorded at cOpenNMR an infrastructure facility funded by the Novo

Nordisk Foundation (NNF18OC0032996). The authors would like to thank the Biophysics Platform—Protein Structure and Function Program from The Novo Nordisk Foundation Center for Protein Research, University of Copenhagen, for performing SECMALS measurements. Novo Nordisk Foundation Center for Protein Research is supported financially by the Novo Nordisk Foundation (NNF14CC0001). Mass spectrometry analyses were performed by the Proteomics Research Infrastructure (PRI) at the University of Copenhagen (UCPH), supported by the Novo Nordisk Foundation (NNF) (grant agreement number NNF19SA0059305).

Author contributions

K.R. and S.B.M. conducted *in vitro* characterization of purified MSBP1 constructs. P.S.T. conducted SAXS experiments. P.S.T. and K.R. performed data analysis. S.B.M. and K.H. conducted proteomics analysis of sorghum seedlings. R.O.F. and V.T. conducted protoplast transformations and microscopy. K.R., S.B.M., R.O.F., and T.L. wrote and edited the manuscript. All authors revised and approved the manuscript.

Supplementary Data

Supplementary Data is available at *PCP* online.

Conflict of Interest

The authors declare no competing interests.

Funding

This work was supported by a Sapere Aude Starting Grant from the Independent Research Fund Denmark (7026-00041B) and a Novo Nordisk Foundation Emerging Investigator Grant (NNF19OC0055356) to T.L. R.O.F. has received funding from the European Union's Horizon 2020 research and innovation programme under the Marie Sklodowska-Curie (grant agreement No 101066828).

Data Availability

Proteomics data are available from ProteomeXchange via the PRIDE partner repository with the dataset identifier PXD058939.

References

Agee, A.E., Surpin, M., Sohn, E.J., Girke, T., Rosado, A., Kram, B.W., et al. (2010) Modified vacuole phenotype1 is an *Arabidopsis myrosinase*-associated protein involved in endomembrane protein trafficking. *Plant Physiol.* 152: 120–132.

Ahmed, I.S., Rohe, H.J., Twist, K.E. and Craven, R.J. (2010) Pgrmc1 (progesterone receptor membrane component 1) associates with epidermal growth factor receptor and regulates Erlotinib sensitivity*. *J. Biol. Chem.* 285: 24775–24782.

Bassard, J.-E. and Laursen, T. (2019) Chapter one - molecular snapshots of dynamic membrane-bound metabolons. In *Methods in Enzymology*, edited by Schmidt-Dannert, C. and Quin, M.B., pp. 1–27. Academic Press.

Bassard, J.-E., Mutterer, J., Duval, F. and Werck-Reichhart, D. (2012) A novel method for monitoring the localization of cytochromes P450 and other endoplasmic reticulum membrane associated proteins: a tool for investigating the formation of metabolons. *FEBS J.* 279: 1576–1583.

Benjamini, Y. and Hochberg, Y. (1995) Controlling the false discovery rate: a practical and powerful approach to multiple testing. *J. R. Stat. Soc. Ser. B Methodol.* 57: 289–300.

Berka, M., Luklová, M., Dufková, H., Berková, V., Novák, J., Saiz-Fernández, I., et al. (2020) Barley root proteome and metabolome in response to Cytokinin and abiotic stimuli. *Front. Plant Sci.* 11: 590337.

Cabrera, J., Barcala, M., Fenoll, C. and Escobar, C. (2014) Transcriptomic signatures of transfer cells in early developing nematode feeding cells of Arabidopsis focused on auxin and ethylene signaling. *Front. Plant Sci.* 5: 107.

Cahill, M.A., Jazayeri, J.A., Kovacevic, Z. and Richardson, D.R. (2016) PGRMC1 regulation by phosphorylation: potential new insights in controlling biological activity. *Oncotarget* 7: 50822–50827.

Chen, Y.-J., Knupp, J., Arunagiri, A., Haataja, L., Arvan, P. and Tsai, B. (2021) PGRMC1 acts as a size-selective cargo receptor to drive ER-phagic clearance of mutant prohormones. *Nat. Commun.* 12: 5991.

Demichev, V., Messner, C.B., Vernardis, S.I., Lilley, K.S. and Ralser, M. (2020) DIA-NN: neural networks and interference correction enable deep proteome coverage in high throughput. *Nat. Methods* 17: 41–44.

Demichev, V., Szyrwiel, L., Yu, F., Teo, G.C., Rosenberger, G., Niewienda, A., et al. (2022) Dia-PASEF data analysis using FragPipe and DIA-NN for deep proteomics of low sample amounts. *Nat. Commun.* 13: 3944.

Ferrero, S., Grados-Torrez, R.E., Leivar, P., Antolin-Llovera, M., Lopez-Iglesias, C., Cortadellas, N., et al. (2015) Proliferation and morphogenesis of the endoplasmic reticulum driven by the membrane domain of 3-hydroxy-3-methylglutaryl coenzyme a reductase in plant cells. *Plant Physiol.* 168: 899–914.

Frankenfield, A.M., Ni, J., Ahmed, M. and Hao, L. (2022) Protein contaminants matter: building universal protein contaminant libraries for DDA and DIA proteomics. *J. Proteome Res.* 21: 2104–2113.

Galmozzi, A., Kok, B.P., Kim, A.S., Montenegro-Burke, J.R., Lee, J.Y., Spreafico, R., et al. (2019) PGRMC2 is an intracellular haem chaperone critical for adipocyte function. *Nature* 576: 138–142.

Gerault, M.A., Camoin, L. and Granjeaud, S. (2024) DIAgui: a shiny application to process the output from DIA-NN. *Bioinform Adv.* 4: vbae001.

Gou, M., Ran, X., Martin, D.W. and Liu, C.-J. (2018) The scaffold proteins of lignin biosynthetic cytochrome P450 enzymes. *Nat. Plants* 4: 299–310.

Han, J., Ma, K., Li, H., Su, J., Zhou, L., Tang, J., et al. (2022) All-in-one: a robust fluorescent fusion protein vector toolbox for protein localization and BiFC analyses in plants. *Plant Biotechnol. J.* 20: 1098–1109.

Hehenberger, E., Eitel, M., Fortunato, S.A.V., Miller, D.J., Keeling, P.J. and Cahill, M.A. (2020) Early eukaryotic origins and metazoan elaboration of MAPR family proteins. *Mol. Phylogenet. Evol.* 148: 106814.

Hopkins, J.B., Gillilan, R.E. and Skou, S. (2017) BioXTAS RAW: improvements to a free open-source program for small-angle X-ray scattering data reduction and analysis. *J. Appl. Crystallogr.* 50: 1545–1553.

Jumper, J., Evans, R., Pritzel, A., Green, T., Figurnov, M., Ronneberger, O., et al. (2021) Highly accurate protein structure prediction with AlphaFold. *Nature* 596: 583–589.

Kabe, Y., Nakane, T., Koike, I., Yamamoto, T., Sugiura, Y., Harada, E., et al. (2016) Haem-dependent dimerization of PGRMC1/Sigma-2 receptor facilitates cancer proliferation and chemoresistance. *Nat. Commun.* 7: 11030.

Kabe, Y., Koike, I., Yamamoto, T., Hirai, M., Kanai, A., Furuhata, R., et al. (2021) Glycyrrhizin derivatives suppress cancer chemoresistance by inhibiting progesterone receptor membrane component 1. *Cancers (Basel)* 13: 3265.

Kaluka, D., Batabyal, D., Chiang, B.-Y., Poulos, T.L. and Yeh, S.-R. (2015) Spectroscopic and mutagenesis studies of human PGRMC1. *Biochemistry* 54: 1638–1647.

Karimi, M., Inze, D. and Depicker, A. (2002) Gateway vectors for agrobacterium-mediated plant transformation. *Trends Plant Sci.* 7: 193–195.

Kikhney, A.G. and Svergun, D.I. (2015) A practical guide to small angle X-ray scattering (SAXS) of flexible and intrinsically disordered proteins. *FEBS Lett.* 589: 2570–2577.

Kimura, I., Yoshioka, M., Konishi, M., Miyake, A. and Itoh, N. (2005) Neudesin, a novel secreted protein with a unique primary structure and neurotrophic activity. *J. Neurosci. Res.* 79: 287–294.

Kimura, I., Nakayama, Y., Konishi, M., Kobayashi, T., Mori, M., Ito, M., et al. (2010) Neuferricin, a novel extracellular heme-binding protein, promotes neurogenesis. *J. Neurochem.* 112: 1156–1167.

Korkhov, V.M. and Zuber, B. (2009) Direct observation of molecular arrays in the organized smooth endoplasmic reticulum. *BMC Cell Biol.* 10: 59.

Kuhn, H., Küster, H. and Requena, N. (2010) Membrane steroid-binding protein 1 induced by a diffusible fungal signal is critical for mycorrhization in Medicago truncatula. *New Phytol.* 185: 716–733.

Langfelder, P. and Horvath, S. (2008) WGCNA: an R package for weighted correlation network analysis. *BMC Bioinformatics* 9: 559.

Laursen, T., Borch, J., Knudsen, C., Bavishi, K., Torta, F., Martens, H.J., et al. (2016) Characterization of a dynamic metabolon producing the defense compound dhurrin in sorghum. *Science* 354: 890–893.

Laursen, T., Lam, H.Y.M., Sørensen, K.K., Tian, P., Hansen, C.C., Groves, J.T., et al. (2021) Membrane anchoring facilitates colocalization of enzymes in plant cytochrome P450 redox systems. *Commun. Biol.* 4: 1057.

Lee, S.C., Knowles, T.J., Postis, V.L.G., Jamshad, M., Parslow, R.A., Lin, Y.-P., et al. (2016) A method for detergent-free isolation of membrane proteins in their local lipid environment. *Nat. Protoc.* 11: 1149–1162.

Lee, S.K., Kweon, Y.C., Lee, A.R., Lee, Y.Y. and Park, C.Y. (2022) Metastasis enhancer PGRMC1 boosts store-operated Ca2+ entry by uncoiling Ca2+ sensor STIM1 for focal adhesion turnover and actomyosin formation. *Cell Rep.* 38: 110281.

Lemoine, F., Correia, D., Lefort, V., Doppelt-Azeroual, O., Mareuil, F., Cohen-Boulakia, S., et al. (2019) NGPhylogeny.fr: new generation phylogenetic services for non-specialists. *Nucleic Acids Res.* 47: W260–W265.

Manalastas-Cantos, K., Konarev, P.V., Hajizadeh, N.R., Kikhney, A.G., Petoukhov, M.V., Molodenskiy, D.S., et al. (2021) ATSAS 3.0: expanded functionality and new tools for small-angle scattering data analysis. *J. Appl. Crystallogr.* 54: 343–355.

McGuire, M.R., Mukhopadhyay, D., Myers, S.L., Mosher, E.P., Brookheart, R.T., Kammers, K., et al. (2021) Progesterone receptor membrane component 1 (PGRMC1) binds and stabilizes cytochromes P450 through a heme-independent mechanism. *J. Biol. Chem.* 297: 101316.

Meyer, C., Schmid, R., Scriba, P.C. and Wehling, M. (1996) Purification and partial sequencing of high-affinity progesterone-binding site(s) from porcine liver membranes. *Eur. J. Biochem.* 239: 726–731.

Mirdita, M., Schütze, K., Moriwaki, Y., Heo, L., Ovchinnikov, S. and Steinegger, M. (2022) ColabFold: making protein folding accessible to all. *Nat. Methods* 19: 679–682.

Mostafa, I., Yoo, M.J., Zhu, N., Geng, S., Dufresne, C., Abou-Hashem, M., et al. (2017) Membrane proteomics of Arabidopsis glucosinolate mutants cyp79B2/B3 and myb28/29. *Front. Plant Sci.* 8: 534.

Nelson, B.K., Cai, X. and Nebenfuhr, A. (2007) A multicolored set of in vivo organelle markers for co-localization studies in Arabidopsis and other plants. *Plant J.* 51: 1126–1136.

Niu, L., Zhang, H., Wu, Z., Wang, Y., Liu, H., Wu, X., et al. (2018) Modified TCA/acetone precipitation of plant proteins for proteomic analysis. *PLoS One* 13: e0202238.

Perez-Riverol, Y., Bai, J., Bandla, C., Garcia-Seisdedos, D., Hewapathirana, S., Kamatchinathan, S., et al. (2022) The pride database resources in 2022: a hub for mass spectrometry-based proteomics evidences. *Nucleic Acids Res.* 50: D543–D552.

Piel, R.B. III, Shiferaw, M.T., Vashisht, A.A., Marcero, J.R., Praissman, J.L., Phillips, J.D., et al. (2016) A novel role for progesterone receptor membrane component 1 (PGRMC1): a partner and regulator of ferrochelatase. *Biochemistry* 55: 5204–5217.

Ritchie, M.E., Phipson, B., Wu, D., Hu, Y., Law, C.W., Shi, W., et al. (2015) Limma powers differential expression analyses for RNA-sequencing and microarray studies. *Nucleic Acids Res.* 43: e47.

Rohe, H.J., Ahmed, I.S., Twist, K.E. and Craven, R.J. (2009) PGRMC1 (progesterone receptor membrane component 1): a targetable protein with multiple functions in steroid signaling, P450 activation and drug binding. *Pharmacol. Ther.* 121: 14–19.

Ryu, C.S., Klein, K. and Zanger, U.M. (2017) Membrane associated progesterone receptors: promiscuous proteins with pleiotropic functions - focus on interactions with cytochromes P450. *Front. Pharmacol.* 8: 159–159.

Saito, C., Uemura, T., Awai, C., Tominaga, M., Ebine, K., Ito, J., et al. (2011) The occurrence of 'bulbs', a complex configuration of the vacuolar membrane, is affected by mutations of vacuolar SNARE and phospholipase in Arabidopsis. *Plant J.* 68: 64–73.

Sandor, A., Fricker, M.D., Kriechbaumer, V. and Sweetlove, L.J. (2021) IntEResting structures: formation and applications of organized smooth endoplasmic reticulum in plant cells. *Plant Physiol.* 185: 550–561.

Sandor, A., Samalova, M., Brandizzi, F., Kriechbaumer, V., Moore, I., Fricker, M.D., et al. (2024) Characterization of intracellular membrane structures derived from a massive expansion of endoplasmic reticulum (ER) membrane due to synthetic ER-membrane-resident polyproteins. *J. Exp. Bot.* 75: 45–59.

Schwanhausser, B., Busse, D., Li, N., Dittmar, G., Schuchhardt, J., Wolf, J., et al. (2011) Global quantification of mammalian gene expression control. *Nature* 473: 337–342.

Segami, S., Makino, S., Miyake, A., Asaoka, M. and Maeshima, M. (2014) Dynamics of vacuoles and H+-pyrophosphatase visualized by monomeric green fluorescent protein in Arabidopsis: artifactual bulbs and native intravacuolar spherical structures. *Plant Cell* 26: 3416–3434.

Shi, Q.-M., Yang, X., Song, L. and Xue, H.-W. (2011) Arabidopsis MSBP1 is activated by HY5 and HYH and is involved in Photomorphogenesis and Brassinosteroid sensitivity regulation. *Mol. Plant* 4: 1092–1104.

von Sivers, L., Jaspar, H., Johst, B., Roese, M., Bitterlich, M., Franken, P., et al. (2019) Brassinosteroids affect the Symbiosis between the AM fungus *Rhizoglomus irregularis* and Solanaceous host plants. *Front. Plant Sci.* 10: 571.

Skinner, S.P., Fogh, R.H., Boucher, W., Ragan, T.J., Mureddu, L.G. and Vuister, G.W. (2016) CcpNmr AnalysisAssign: a flexible platform for integrated NMR analysis. *J. Biomol. NMR* 66: 111–124.

Smith, A.A.A., Autzen, H.E., Laursen, T., Wu, V., Yen, M., Hall, A., et al. (2017) Controlling styrene maleic acid lipid particles through raft. *Biomacromolecules* 18: 3706–3713.

Song, J., Vinarov, D.A., Tyler, E.M., Shahan, M.N., Tyler, R.C. and Markley, J.L. (2004) Letter to the editor: hypothetical protein At2g24940.1 from *Arabidopsis thaliana* has a cytochrome b5 like fold∗. *J. Biomol. NMR* 30: 215–218.

Song, L., Shi, Q.-M., Yang, X.-H., Xu, Z.-H. and Xue, H.-W. (2009) Membrane steroid-binding protein 1 (MSBP1) negatively regulates brassinosteroid signaling by enhancing the endocytosis of BAK1. *Cell Res.* 19: 864–876.

Steenwyk, J.L., Buida, T.J. 3rd, Li, Y., Shen, X.X. and Rokas, A. (2020) ClipKIT: a multiple sequence alignment trimming software for accurate phylogenomic inference. *PLoS Biol.* 18: e3001007.

Strehmel, N., Hoehenwarter, W., Monchgesang, S., Majovsky, P., Kruger, S., Scheel, D., et al. (2017) Stress-related mitogen-activated protein kinases stimulate the accumulation of small molecules and proteins in Arabidopsis thaliana root exudates. *Front. Plant Sci.* 8: 1292.

Thomas, P.D., Ebert, D., Muruganujan, A., Mushayahama, T., Albou, L.P. and Mi, H. (2022) PANTHER: making genome-scale phylogenetics accessible to all. *Protein Sci.* 31: 8–22.

Tria, G., Mertens, H.D.T., Kachala, M. and Svergun, D.I. (2015) Advanced ensemble modelling of flexible macromolecules using X-ray solution scattering. *IUCrJ* 2: 207–217.

Trifinopoulos, J., Nguyen, L.T., von Haeseler, A. and Minh, B.Q. (2016) W-IQ-TREE: a fast online phylogenetic tool for maximum likelihood analysis. *Nucleic Acids Res.* 44: W232–W235.

Witzel, K., Matros, A., Møller, A.L.B., Ramireddy, E., Finnie, C., Peukert, M., et al. (2018) Plasma membrane proteome analysis identifies a role of barley membrane steroid binding protein in root architecture response to salinity. *Plant Cell Environ.* 41: 1311–1330.

Wu, T.M., Lin, K.C., Liau, W.S., Chao, Y.Y., Yang, L.H., Chen, S.Y., et al. (2016) A set of GFP-based organelle marker lines combined with DsRed-based gateway vectors for subcellular localization study in rice (*Oryza sativa* L.). *Plant Mol. Biol.* 90: 107–115.

Yang, X.-H., Xu, Z.-H. and Xue, H.-W. (2005) Arabidopsis membrane steroid binding protein 1 is involved in inhibition of cell elongation. *Plant Cell* 17: 116–131.

Yang, X., Song, L. and Xue, H.-W. (2008) Membrane steroid binding protein 1 (MSBP1) stimulates tropism by regulating vesicle trafficking and auxin redistribution. *Mol. Plant* 1: 1077–1087.

You, J.H., Lee, J. and Roh, J.-L. (2021) PGRMC1-dependent lipophagy promotes ferroptosis in paclitaxel-tolerant persister cancer cells. *J. Exp. Clin. Cancer Res.* 40: 350.

Yu, G., Wang, L.G., Han, Y. and He, Q.Y. (2012) clusterProfiler: an R package for comparing biological themes among gene clusters. *OMICS* 16: 284–287.

Zhang, X., Smits, A.H., van Tilburg, G.B., Ovaa, H., Huber, W. and Vermeulen, M. (2018) Proteome-wide identification of ubiquitin interactions using UbIA-MS. *Nat. Protoc.* 13: 530–550.

Zhu, Z.X., Ye, H.B., Xuan, Y.H. and Yao, D.N. (2014) Overexpression of a SNARE protein AtBS14b alters BR response in Arabidopsis. *Bot. Stud.* 55: 55.

Plant and Cell Physiology, 2026, 67(3),315–328. https://doi.org/10.1093/pcp/pcaf160, Advance Access publication on 4 December 2025, available online at https://academic.oup.com/pcp
Regular Paper